The EMBO Journal (2006) 25, 4897–4908 | © 2006 European Molecular Biology Organization | All Rights Reserved 0261-4189/06
www.embojournal.org

THE EMBO JOURNAL

Dynein-mediated pulling forces drive rapid mitotic spindle elongation in *Ustilago maydis*

Gero Fink[1], Isabel Schuchardt[1], Julien Colombelli[2], Ernst Stelzer[2] and Gero Steinberg[1,*]

[1]Max-Planck-Institut für terrestrische Mikrobiologie, Marburg, Germany and [2]European Molecular Biology Laboratory, Heidelberg, Germany

Spindle elongation segregates chromosomes and occurs in anaphase, an essential step in mitosis. Dynein-mediated pulling forces position the spindle, but their role in anaphase is a matter of debate. Here, we demonstrate that dynein is responsible for rapid spindle elongation in the model fungus *Ustilago maydis*. We show that initial slow elongation is supported by kinesin-5, which is located in the spindle mid-zone. When the spindle reaches ~2 μm in length, the elongation rate increases four-fold. This coincides with the appearance of long and less-dynamic microtubules (MTs) at each pole that accumulate dynein at their tips. Laser-mediated nanosurgery revealed that these MTs exert pulling forces in control cells, but not in dynein mutants. In addition, dynein mutants undergo initial slow anaphase, but fail to establish less-dynamic MTs and do not perform rapid spindle elongation, suggesting that dynein drives anaphase B. This is most likely mediated by cortical sliding of astral MTs along stationary dynein, which is off-loaded from the MT plus-end to the cortex.

The EMBO Journal (2006) **25,** 4897–4908. doi:10.1038/sj.emboj.7601354; Published online 5 October 2006
Subject Categories: cell cycle
Keywords: anaphase B; dynein; kinesin-5; microsurgery; plant pathogen

Introduction

In mitosis, chromosomes are segregated between dividing cells. Segregation is achieved by the highly ordered mitotic spindle, which mainly consists of microtubules (MTs) to which chromosomes attach. MTs also participate in force generation during pole ward movement of chromosomes in anaphase A and spindle elongation in anaphase B that is mainly mediated by molecular motors (Barton and Goldstein, 1996). In general, these mechanoenzymes obtain energy by hydrolyzing ATP for their work along the cytoskeleton, but they also participate in regulating MT assembly and disassembly, thereby supporting spindle dynamics (Gadde and Heald, 2004; Sharp and Rogers, 2004).

*Corresponding author. Max-Planck-Institut für terrestrische Mikrobiology, Karl-von-Frisch-Straße, 35043 Marburg, Germany.
Tel.: +49 6421 178 530; Fax: +49 6421 178 599;
E-mail: Gero.Steinberg@staff.uni-marburg.de

Received: 31 March 2006; accepted: 22 August 2006; published online: 5 October 2006

MT-associated motors can be classified as kinesins and dyneins (Hirokawa, 1998). While dyneins move their cargo towards the minus-ends of MTs (Karki and Holzbaur, 1999), the function of kinesins is more divers, as most motors walk towards plus-ends, whereas some C-terminal kinesins transport cargo towards minus-ends (Noda *et al*, 2001) or even have lost their transport function, but modify MT dynamics (Moore and Wordeman, 2004; Helenius *et al*, 2006). Numerous studies in various organisms have demonstrated that the bipolar kinesin-5 supports spindle elongation; kinesin-5 is thought to act on MTs in the mid-zone of the spindle, thereby supporting spindle integrity and elongation (Hagan and Yanagida, 1992; Kashina *et al*, 1997; Sharp *et al*, 1999).

In addition, laser-mediated MT surgery experiments have provided evidence for the existence of external forces applied on the spindle (Aist and Berns, 1981; Aist *et al*, 1991, 1993; Grill *et al*, 2001). These forces are most likely exerted via astral MTs that emanate from the spindle poles and contact the cellular cortex (Grill and Hyman, 2005). A good candidate for the responsible motor is cytoplasmic dynein. Dynein is found at the cellular cortex of animal cells and is thought to participate in rotation and positioning of the spindle by pulling on astral MTs (O'Connell and Wang, 2000; Gönczy, 2002). Moreover, dynein supports spindle elongation in anaphase B in *Drosophila melanogaster* (Sharp *et al*, 2000), but no such role was seen in PTK and HeLa cells (Vaisberg *et al*, 1993; Zhu *et al*, 2005). However, in these cells, such a role of dynein might be hidden under the pleiotropic consequences of dynein inhibition.

In the yeast fungus *Saccharomyces cerevisiae,* dynein also supports spindle positioning (Yeh *et al*, 1995). The minus-motor accumulates at astral MT plus-ends, from where it is off-loaded to the cortex and becomes activated, and, consequently, pulls on the spindle pole (Lee *et al*, 2003; Sheeman *et al*, 2003). However, dynein neither supports spindle elongation in this fungus (Saunders *et al*, 1995; Yeh *et al*, 1995) nor participates in spindle elongation in *Schizosaccharomyces pombe* (Yamamoto *et al*, 1999), and no pulling forces are applied on astral MTs (Khodjakov *et al*, 2004; Tolic-Norrelykke *et al*, 2004). Thus, anaphase appears to be independent of cytoplasmic dynein in these yeasts.

Here, we study forces in spindle elongation in *Ustilago maydis*. This fungal model organism provides several technical advantages, such as excellent molecular genetic and live-cell-imaging techniques and an interesting biology that in many respects is very closely related to that of animal cells, for example, the dynein-dependent removal of the nuclear envelope during 'open mitosis' (Straube *et al*, 2005). We describe that early spindle elongation is supported by kinesin-5 and that at the transition to rapid spindle elongation, dynein appears at plus-ends of astral MTs, exerts force on the spindle poles by mediating sliding of astral MTs along the cortex.

Results

Rapid spindle elongation coincides with the appearance of long astral MTs

Mitosis in *U. maydis* begins with the migration of the spindle pole bodies into the daughter cell and the subsequent removal of the nuclear envelope (Straube *et al*, 2005). The spindle establishes in the daughter cell, and chromosomes are segregated by rapid elongation in anaphase (Figure 1A). We monitored the pole-to-pole distance over time of 35 spindles in strain FB2GT that contained an additional copy of green fluorescent protein (GFP)-α-tubulin (Steinberg *et al*, 2001) and in FB2R$_3$Dyn1_GT that contains the endogenous copy of the N-terminal half of dynein heavy chain tagged with triple red fluorescent protein (RFP; for all strains see Table I). Overlapping spindle elongation graphs were aligned and the average elongation velocity was determined by linear regression. Anaphase started with a slow phase, during which the spindle elongated at $1.23 \pm 0.18\,\mu m\,min^{-1}$ (Figure 1B). In this phase chromosomes became separated (Figure 1C; DNA stained with histone-4 fused to cyan fluorescence protein is given in red, and the spindles labeled with yellow fluorescent protein to α-tubulin in green; strain FB1H4C_YT) (Straube *et al*, 2005), and we therefore refer to it as anaphase A. Slow spindle elongation occurred in the daughter cell, and the spindle remained almost immobile, with only occasional short rotational motions (see below). When the spindle reached a length of 1.5–2.0 μm, the elongation rate increased about four-fold to $5.34 \pm 0.14\,\mu m\,min^{-1}$ (anaphase B; Figure 1B). This coincided with the sudden appearance of numerous long astral MTs at both spindle poles (Figure 1D; see Supplementary Movie 1). The two most distal MTs had a length of 2–7 μm, extended toward both cell poles (Figure 1D, arrowheads), and remained in close contact with the cell cortex, while the spindle elongated or rapidly moved bidirectionally.

Kinesin-5 mediates slow spindle elongation

The low spindle elongation rate in early anaphase in *U. maydis* corresponded well with rates observed in *S. cerevisiae* and *S. pombe* ($1–1.6\,\mu m\,min^{-1}$; Hagan and Yanagida, 1990; Yeh *et al*, 1995). In these yeasts, anaphase is driven by outward forces generated by kinesin-5 motors (Hagan and Yanagida, 1990; Hoyt *et al*, 1992). The *U. maydis* genome encodes for a kinesin-5 protein (Schuchardt *et al*, 2005) with 54 and 47% identity to the motor domains from BimC from *Apergillus nidulans* and Eg5 from *Xenopus laevis*, respectively. All these kinesin-5 motors are predicted to contain a putative phosphorylation site, known as the bimC box (Drummond and Hagan, 1998; Figure 2A).

We localized kinesin-5 of *U. maydis* by using endogenous kinesin-5 tagged with three green fluorescent proteins (GFP$_3$-

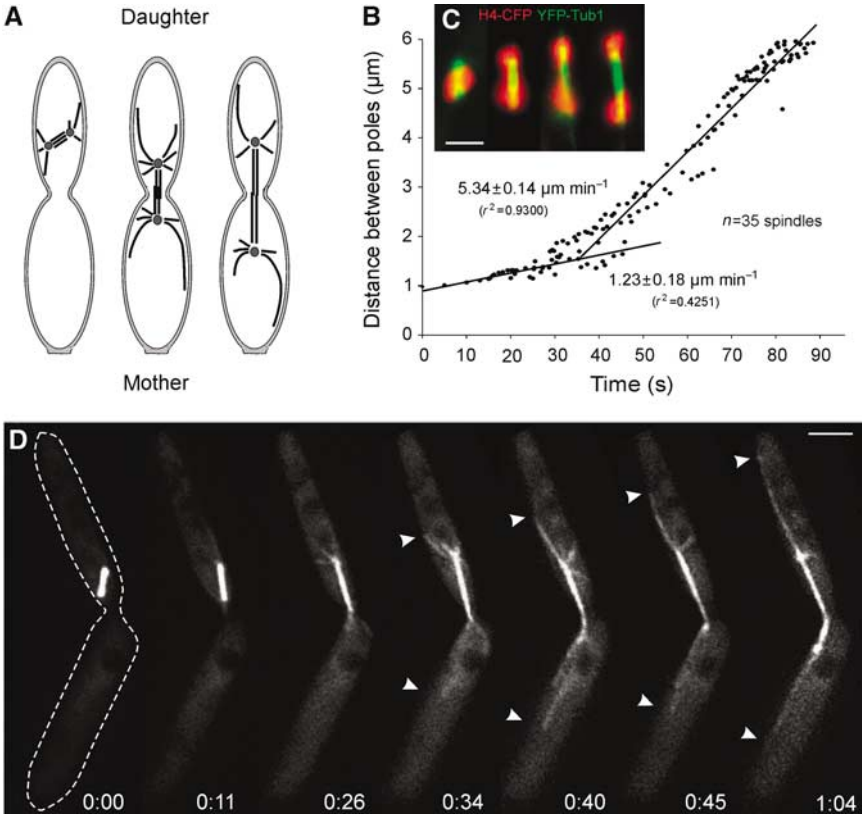

Figure 1 Spindle elongation in anaphase in *U. maydis*. (**A**) Overview of late mitotic stages in *U. maydis*. Anaphase is initiated in the daughter cell, and spindle elongation segregates the chromosomes into the daughter and mother cells (modified from Steinberg *et al*, 2001). (**B**) Linear regression analysis of spindle elongation during anaphase. Spindle elongation starts with a slow phase, but rapidly increases when spindles reach a length of 1.5–2 μm. The graph is based on the analysis of 35 spindles that were aligned; each spindle was observed for 30 s. (**C**) DNA separation in strain FB1H4C_YT, which expresses a CFP-H4 fusion protein (red) and YFP-α-tubulin (green). Initial steps of chromosomes separation are categorized and stages 1–4 correspond to Figure 5C. Note that images were taken from different spindles. Bar: 2 μm. (**D**) Time-lapse fluorescence microscopy of spindle elongation and spindle positioning in *U. maydis* strain FB2GT using GFP-α-tubulin-labeled MTs. Note that rapid spindle elongation coincides with the appearance of long astral MTs at both spindle poles (arrowheads) that slide along the cortex while the spindle elongates. The edge of the cell is indicated at time 0 by a dotted line. Elapsed time in minutes and seconds is indicated. Bar: 3 μm.

Table I Strains and plasmids used in this study

Strain or plasmid	Genotype	Reference
FB1GT	*a1b1*/potefGFPTub1	Steinberg *et al* (2001)
FB2GT	*a2b2*/potefGFPTub1	Straube *et al* (2001)
$FB2R_3Dyn1\_GT$	*a2b2* P*dyn1-3xmrfp-dyn1*, nat^R/potefGFPTub1	This study
FB1H4C_YT	*a1b1*/pH4CFP/pYFPTub1	Straube *et al* (2005)
$FB2G_3Kin5\_RT$	*a2b2* P*kin5-3xgfp-kin5*, hyg^R/potefRFPTub1	This study
$AB33Kin5^{ts}\_GT$	*a2* P*narbW2* P*narbE* ,ble^R P*kin5-kin5*^{R210K}, hyg^R/potefGFPTub1	This study
$FB1Kin5^{ts}$_Tub2G	*a1b1* P*kin5-kin5*^{R210K}, hyg^R/potefTub2GFP	This study
FB2rGFPTub1	*a2b2*/prGFPTub1	Steinberg *et al* (2001)
$FB1Dyn2^{ts}\_GT$	*a1b1* P*dyn2-dyn2*^{ts}, nat^R/potefGFPTub1	Adamikova *et al* (2004)
FB2rDya1_GT	*a2b2* P*crg-dya1*, ble^R/potefGFPTub1	This study
FB1rDyn2_GT	*a1b1* P*crg-dyn2*, ble^R/potefGFPTub1	This study
$FB1Dyn2^{ts}$_$Kin5^{ts}$_GT	*a1b1* P*dyn2-dyn2*^{ts}, nat^R P*kin5-kin5*^{R210K}, hyg^R/potefGFPTub1	This study
$FB2G_2Dyn1\_RT$	*a2b2* P*dyn1-2xgfp-dyn1*, hyg^R/pRFPTub1	Straube *et al* (2005)
potefTub2GFP	P*otef-tub2gfp*, cbx^R	Straube *et al* (2003)
potefGFPTub1	P*otef-gfp-tub1*, cbx^R	Steinberg *et al* (2001)
pYFPTub1	P*otef-yfp-tub1*, cbx^R	Straube *et al* (2005)
prGFPTub1	P*crg-gfp-tub1*, cbx^R	Steinberg *et al* (2001)
pRFPTub1	P*otef-mrfp-tub1*, cbx^R	Straube *et al* (2005)
pH4CFP	P*his4-his4-3xcfp*, cbx^R	Straube *et al* (2005)

A, *b*, mating type loci; P, promoter; -, fusion; hyg^R, hygromycin resistance; ble^R, phleomycin resistance; nat^R, nourseothricin resistance; cbx^R, carboxin resistance; /, ectopically integrated; *otef*, constitutive promoter; *nar*, conditional nitrate reductase promoter; *crg*, conditional arabinose-induced promoter; *E1*, *W2*, genes of the *b* mating type locus; *gfp*, enhanced green fluorescent protein; *cfp*, cyan-shifted fluorescent protein; *yfp*, yellow-shifted fluorescent protein; *mrfp*, monomeric red fluorescent protein; *tub1*, α-tubulin; *tub2*, γ-tubulin; *dyn1*, N-terminal half of the dynein heavy chain; *dyn2*, C-terminal half of the dynein heavy chain; $dyn2^{ts}$, temperature-sensitive allele of *dyn2*; *his4*, histone 4; *kin5*, kinesin-5/BimC-like kinesin; $kin5^{ts}$, temperature-sensitive allele of *kin5*.

Kin5). GFP_3-Kin5 localized along the length of the spindle in anaphase A (<2 μm; Figure 2B) and concentrated in the spindle mid-zone and the spindle poles in anaphase B (spindle length 2–8 μm; Figure 2B, arrowheads; strain $FB2G_3Kin5\_RT$). When the spindles reached a length of ~7 μm, GFP_3-Kin5 was no longer concentrated in the mid-zone (Figure 2B, asterisk), but traces of GFP_3-Kin5 were still located over the length of the spindle (Figure 2B, lowest panel). The role of kinesin-5 in spindle elongation was investigated by introducing a point mutation (R210K) into the endogenous *kin5*. This mutation corresponds to an exchange within the motor domain in the temperature-sensitive *cin8-3* allele in *S. cerevisiae* (Gheber *et al*, 1999). At 16°C, cells of strain $AB33Kin5^{ts}\_GT$ grew normally (Figure 2C), but at restrictive temperature (32°C for 4 h) an accumulation of mitotic cells was found (Figure 2D). These cells contained short bipolar spindles, as illustrated by the labeling of the spindle pole bodies with γ-tubulin-GFP (Figure 2E; strain $FB1Kin5^{ts}$_Tub2G). Surprisingly, only 33.6% ($n=380$ cells) showed this phenotype (4.98%, $n=321$ cells in control) and $kin5^{ts}$ mutants in liquid culture continued to grow (not shown). This finding was unexpected, as the corresponding $cin8^{ts}$ mutants in *S. cerevisiae* almost completely arrested in mitosis (Hoyt *et al*, 1992). The reason for this discrepancy between *U. maydis* and *S. cerevisiae* is not yet known, and it remains to be seen whether the mutation R210K in *kin5* is 'not tight' or whether other motors participate in initial spindle elongation in *U. maydis*. However, we consider it likely that kinesin-5 participates in supporting initial spindle elongation, most likely by generating outward forces within the midzone.

External pulling forces are applied on the anaphase spindle

As mentioned above, anaphase A in *U. maydis* is followed by a phase of rapid elongation in anaphase B. The spindle occasionally ($n=3$) broke during anaphase B in *U. maydis* (Figure 3A, arrow; arrowheads indicate spindle poles; see Supplementary Movie 2), which led to rapid separation of both poles at increased velocity (from 6.0 to 32.5 μm min^{-1}; Figure 3A, arrowheads). These results suggested that external pulling forces act on the spindle in *U. maydis*. To assess the role of astral MTs in force generation, we severed MTs using pulsed laser nanosurgery as previously described (Colombelli *et al*, 2005). A few laser pulses were sufficient to induce astral MT and anaphase spindle dissection inside the focal volume of the beam without affecting the overall cell. Severing the spindle significantly increased the pole separation rate (Figure 3B and D; from 5.9 ± 1.0 μm min^{-1}, $n=14$ to 24.2 ± 9.4 μm min^{-1}, $n=14$; $P<0.0001$; see Supplementary Movie 3), while cytoplasmic irradiation did not effect spindle elongation (Figure 3E; $P=0.2128$). Interestingly, the two halves of the spindle moved pole ward at different rates (Figure 3F; $P=0.0329$), occasionally oscillated and underwent 1–2 pauses of ~4 s before they became positioned at the middle of the daughter or the mother cell (Figure 3C). This behavior of individual spindle poles suggests that counteracting forces are exerted on each pole, which might help to position the spindle poles in late mitosis. In order to investigate whether astral MTs, and in particular the long distal MTs (see Figure 1D, arrowheads) exert forces, leading MTs were cut with the UV laser (Figure 3G; see Supplementary Movie 4). This treatment did not affect the overall organization of the spindle or the MT asters. In 26 out of 31 severed MTs, the generated fragments moved along the cortex towards the cell end (Figure 3G; asterisks indicate ends of a moving fragment; arrow marks the point of dissection; arrowheads indicate spindle poles). The removal of the distal MT, or even all astral MTs visible at a pole, induced an average displacement of the spindle of 1.22 ± 0.46 μm ($n=19$; Figure 3G) before new astral MTs appeared that stabilized the spindle (not shown). In summary, these results demonstrate that astral MTs and in particular the long and

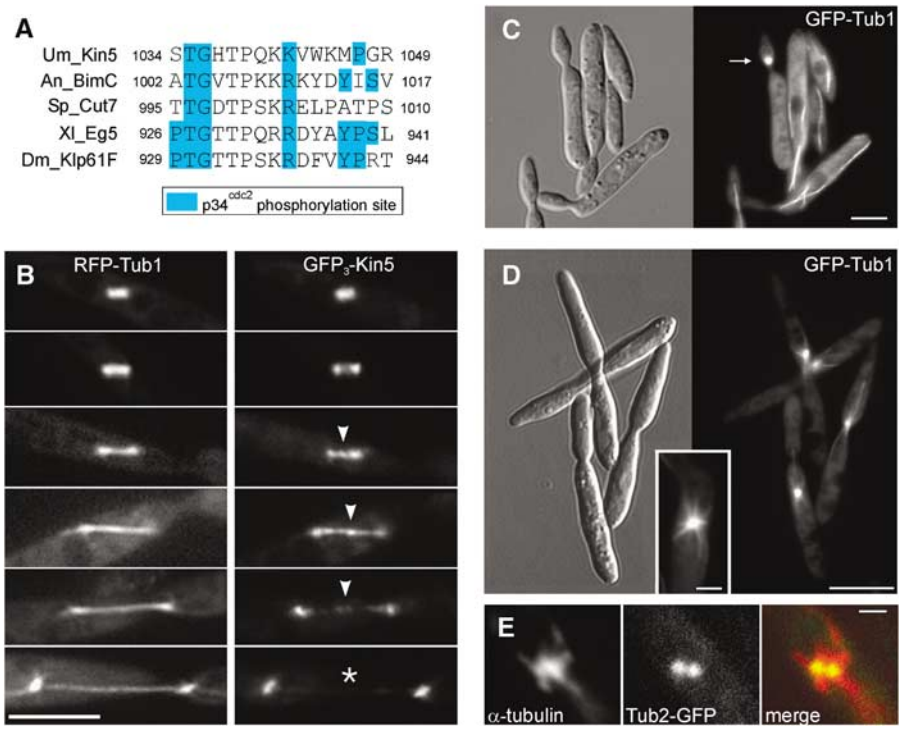

Figure 2 The role and localization of kinesin-5 in anaphase in *U. maydis*. (**A**) Alignment of the bimC-box that represents a putative phosphorylation site (Drummond and Hagan, 1998) in kinesin-5 from *A. nidulans* (BimC), *S. pombe* (Cut7), *X. laevis* (Eg5) and *D. melanogaster* (Klp61F) and *U. maydis* (Kin5). (**B**) Localization of kinesin-5 in the anaphase spindle. DNA encoding a triple GFP tag was fused to the endogenous *kin5* gene of *U. maydis* (GFP_3-Kin5; right series) and expressed in the presence of RFP-α-tubulin (RFP-Tub1, left series). Time-elapsed photomicrographs of the spindles with the functional fluorescent fusion protein are shown. Arrowheads show GFP_3-Kin5 at the spindle mid-zone that leaves the mid-zone at late anaphase (asterisk). Bar: 5 μm. (**C**) Control images of a conditional *kin5*^{ts} mutant grown at permissive temperature (16°C). Arrow indicates a mitotic cell. Bar: 5 μm. (**D**) Photomicrographs of a conditional *kin5*^{ts} mutant grown at restrictive temperature (32°C) illustrating a defect in mitosis. *U. maydis* AB33Kin5^{ts}_GT contains a point mutation that also confers temperature sensitivity to the kinesin-5 of *S. cerevisiae* (Gheber *et al*, 1999). Bars: 10 μm in overview and 2 μm in inset. (**E**) Colocalization of α-tubulin with GFP tagged γ-tubulin in condensed spindles in strain FB1Kin5^{ts}_Tub2G grown at 32°C. Bar: 1 μm.

most-distal MTs apply external forces on the spindle during rapid spindle elongation.

Less-dynamic astral MTs slide along the cellular cortex

In anaphase B, each spindle pole nucleated three to five short astral MTs that showed dynamic instability and transiently contacted the cortex, but did not slide along the cell periphery. In contrast, the long and most-distal MTs were less dynamic, with reduced depolymerization and elongation rates (Figure 4C; $P = 0.0003$ for shrinkage; $P = 0.0425$ for elongation), and they usually were in close contact with the cortex (Figure 4A, see also Figure 1C). Furthermore, speckle analysis of sliding astral MTs in strain FB2rGFPTub1 revealed that GFP-α-tubulin speckles remained constant during motion of distal MTs (Figure 4A and B), demonstrating that the distal MTs indeed slide along the cellular cortex.

Dynein appears at MT ends and exerts force on astral MTs during rapid spindle elongation

Interestingly, dynein that was endogenously labeled with 3 RFPs (RFP_3) at the N-terminus (strain FB2R_3Dyn1_GT) mainly concentrated at the end of these sliding distal MTs (Figure 4D). This suggested a possible function of dynein in cortical MT sliding. We tested this by monitoring mitosis in conditional dynein mutants that expressed GFP-α-tubulin and carried a temperature-sensitive *dyn2* allele (Wedlich-Söldner *et al*, 2002; strain FB1Dyn2^{ts}_GT). Consistent with previous results, these mutants were defective in premitotic nuclear migration (Straube *et al*, 2001, 2005), but formed a spindle in the mother cell (Figure 5A) that could reach a length of up to 8.5 μm (not shown). However, no long and less-dynamic astral MTs were found and astral MTs fail to establish stable contacts with the cortex (see Supplementary Movie 5). This coincided with a slow elongation rate ($1.7 \pm 0.9\,\mu m\,min^{-1}$, $n = 24$; Figure 5B), which corresponded well with the initial rate of elongation in control cells (Figure 5B; not different, $P = 0.8678$). This suggests that rapid anaphase B requires dynein, whereas elongation up to 2 μm is powered by a dynein-independent mechanism that most likely involves kinesin-5 (see above). Indeed, RFP_3-tagged dynein was absent from astral MTs until the spindle reached 1.5–2.0 μm in length (Figure 5D) and only transiently appeared when short spindles underwent rotational motion (Figure 5C, arrow).

In order to get further support for our conclusion that dynein drives spindle elongation, we investigated anaphase in strain FB2rDya1_GT, which contains the endogenous copy of the homolog of the dynactin subunit p150^{glued} under the control of a repressible promoter (Lenz *et al*, 2006). In restrictive conditions, spindles did not migrate into the daughter cell (not shown) and elongated at rates of $1.63 \pm 0.74\,\mu m\,min^{-1}$ ($n = 16$), which was almost identical to the rate found in dynein mutant cells (FB1Dyn2^{ts}_GT; $P = 0.8907$; Figure 5B). In addition, the dynactin mutant and another dynein mutant strain that contains the endogenous *dyn2* under the control of the repressible *crg* promoter

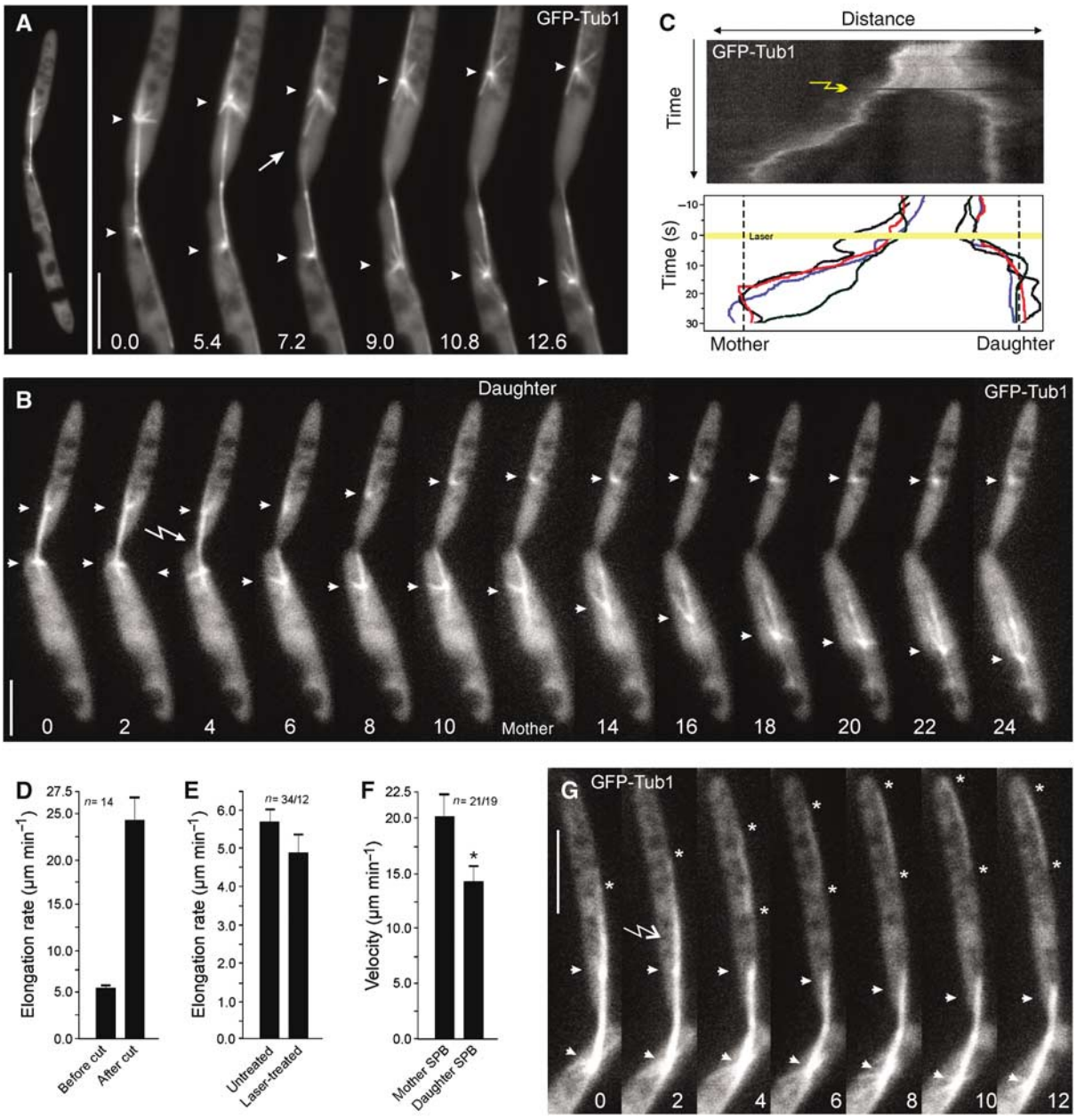

Figure 3 Pulling forces exerted on the spindle via astral MTs. (**A**) Spindle breakage and rapid separation of the spindle poles. Occasionally ($n=3$), breaking of a spindle in anaphase was observed (arrow). Each of the two spindle poles rapidly moved towards the cell poles. Elapsed time is given in seconds. Bars: 10 μm in panel and 5 μm in series. (**B**) Time series illustrating spindle pole separation before (0–4 s) and after UV laser dissection. Elapsed time is given in seconds. Arrow indicates the laser irradiation and arrowheads the spindle poles. Bar: 5 μm. (**C**) Kymograph analysis of spindle pole separation before and after laser dissection. Position of mother and daughter cell is indicated. Lower graph summarizes the behavior of four cut spindles. Laser irrediation is indicated by an arrow (kymograph) or a yellow line (lower graph). Note that spindle halves are positioned shortly after laser dissection (final position indicated by dashed lines). (**D**) Quantitative analysis of spindle pole separation before and after severing of anaphase spindles with a UV laser. (**E**) Control experiments that demonstrate that laser radiation in the cytoplasm does not significantly affect spindle pole separation velocities. (**F**) Quantitative analysis of the average velocity of spindle pole motility after laser dissection. Frequent stops were excluded from the average motility rates. Values given in D, E, F are the mean ± standard deviation. (**G**) Laser dissection of astral MTs (arrow) leads to rapid motility of MT fragments towards the cell pole (asterisks), which was seen in 84% of all cases ($n=31$). Elapsed time is given in seconds, arrowheads indicate the spindle poles. Bar: 5 μm.

(FB1rDyn2_GT) showed abnormal numbers of nuclei, with 42.9 ± 3.4 and 44.5 ± 6.7% of unbudded cells, containing either no or more than one nucleus ($P=0.7533$, $n=3$ experiments 100 cells each). This suggests that dynactin and dynein cooperate in nuclear migration and spindle elongation.

To further strengthen our conclusion that dynein is responsible for force generation in anaphase B, we did nanosurgery experiments on spindles in the temperature-sensitive dynein mutant strain FB1Dyn2^{ts}_GT. In contrast to control cells (Figure 3B), laser-induced dissection of the spindle never led to rapid motility of the spindle halves ($n=10$; Figure 6A; see Supplementary Movie 6). Furthermore, dissection of astral MTs in the dynein mutant did not result in pole ward motion of the MT fragment (Figure 6B and C, arrowheads indicate a severed MT; see Supplementary Movie 7), and no spindle displacement was observed.

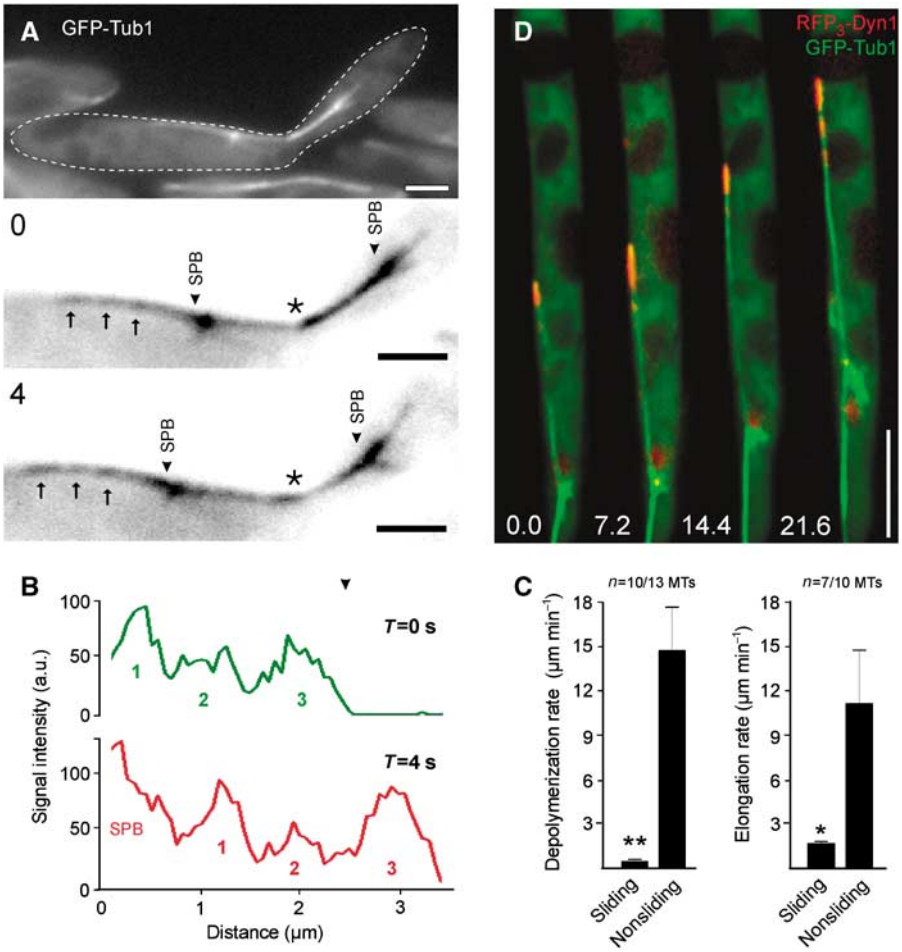

Figure 4 Analysis of the long distal MTs during cortical sliding in *U. maydis*. (**A**) Speckle analysis of a distal MT (GFP-Tub1) during cortical sliding in *U. maydis* FB2rGFPTub1. Spindle pole bodies (SPB) are highlighted by arrowheads. Arrows indicate fluorescent speckles given in black after contrast inversion, asterisks marks the neck region. Elapsed time in seconds (0 or 4 s) is indicated in the upper left. Bars: 2 μm. (**B**) Line-scan analysis of the sliding astral MT depicted in Figure 4A. The three fluorescence intensity peaks (indicated numbers) that represent the moving speckles. The relative position of the peaks remained constant while the MT slides. 'SPB' indicates the strong signal at the spindle pole body. (**C**) Quantitative analysis of elongation and depolymerization rates of sliding versus nonsliding astral MTs. The values given are the mean ± standard deviation. (**D**) Localization of dynein triple labeled at the N-terminus of the heavy chain with red fluorescent protein (RFP_3-Dyn1). RFP_3-Dyn1 (red) strongly accumulated at the plus-end of a GFP-α-tubulin-tagged sliding MT (GFP-Tub1). Note that DNA encoding RFP_3 was fused to the endogenous copy of *dyn1*. Elapsed time in seconds is indicated. Bar: 5 μm.

Taken together, our data suggested that spindle elongation in *U. maydis* is based on the cooperative activity of Kin5 and dynein. In order to gain further support for this notion, we generated a *dyn2*^{ts} *kin5*^{ts} double mutant that carried point mutations in the endogenous genes (FB1Dyn2ts_Kin5ts_GT). Surprisingly, at restrictive conditions these mutants still formed spindles (not shown), but they elongated very slowly ($1.0 \pm 0.77\,\mu m\,min^{-1}$, $n = 11$; different to *dyn2*^{ts} single mutants, *P*: 0.0347; Figure 5B, white bar), again indicating that both motors are required for anaphase in *U. maydis*. These results might also indicate that additional force generating mechanisms exist that drive elongation in the absence of functional dynein and kinesin-5. However, we can currently not exclude that this phenomenon is based on some residual activity of the temperature-sensitive *kin5*^{ts} allele.

The strong dynein accumulation at the distal MT ends is dynamic

The results described above demonstrate that a long astral MT with large amounts of dynein accumulated at its tip exerts force on the spindle. Surprisingly, severing this MT with a laser did not result in much displacement of the spindle (see above), which suggests that additional forces hold the spindle in place. Indeed, we found dynein also at shorter astral MTs (Figure 7A). The strongest signal was always located at the distal MT tip (Figure 7A and B; no. 1), whereas much less dynein was found at laterally oriented MTs (Figure 7A and B; no. 2) or proximal MTs (Figure 7A and B; no. 3). In addition, we found that the distal MT in the mother cell carries more dynein than the one that reaches into the daughter (Figure 7B), which nicely corresponds with the different velocities of spindle halves after laser dissection (see above). The amount of dynein at MT tips correlated with alterations in dynamic instability, as MTs with strong signals (Figure 7A; no. 1) showed increased rescue and catastrophe rates. In addition, these MTs were found to be less dynamic, illustrated by a longer time in pause (Table II). Interestingly, dynein accumulation at the plus-end of distal MTs was variable over time (Figure 7C). Imaging of GFP_2-Dyn1 demonstrated that dynein moved bidirectionally along the

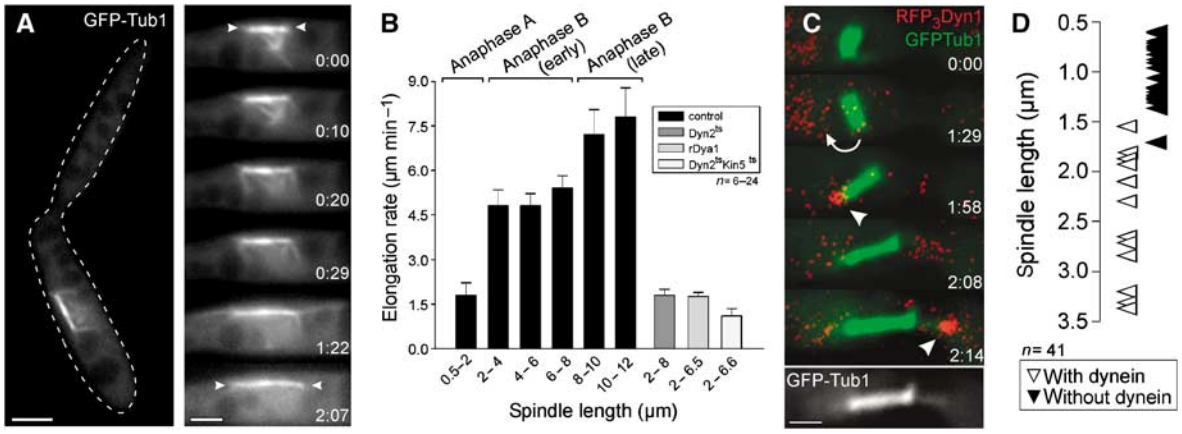

Figure 5 The role of dynein in spindle elongation and chromosome separation in *U. maydis*. (**A**) Fluorescence microscopy of anaphase in temperature-sensitive dynein mutant cells (strain FB1Dyn2^{ts}_GT) containing GFP-α-tubulin-labeled MTs. The edge of the cell is indicated with a dashed line. At restrictive conditions (1–2.5 h at 32°C), the spindle is still able to elongate. Dynamic astral MTs are present, but they neither establish a stable connection with the cortex nor slide along the cell periphery. Arrowheads indicate spindle poles. The elapsed time in seconds is indicated. Bars: 3 μm in overview and 2 μm in series. (**B**) Rate of spindle elongation during different stages of anaphase in control strains (FB1GT and FB2GT; black bars), the temperature-sensitive dynein mutant (FB1Dyn2^{ts}_GT; grey bar), the dynactin (FB2rDya1_GT; light grey bar) and the *dyn2*^{ts} *kin5*^{ts} mutant (FB1Dyn2^{ts}_Kin5^{ts}_GT; white bar). The values are given as mean ± standard error of the mean. (**C**) Dynein and early anaphase spindles in strain FB2R$_3$Dyn1_GT. Note that image pairs were taken using a filter wheel, which results in a short time shift between the images pairs that were merged in the series. Elapsed time in minutes is indicated. Bar: 1 μm. (**D**) Graph depicting the correlation between spindle length and dynein appearance at MT plus-ends. Transient dynein appearance during rotation was ignored.

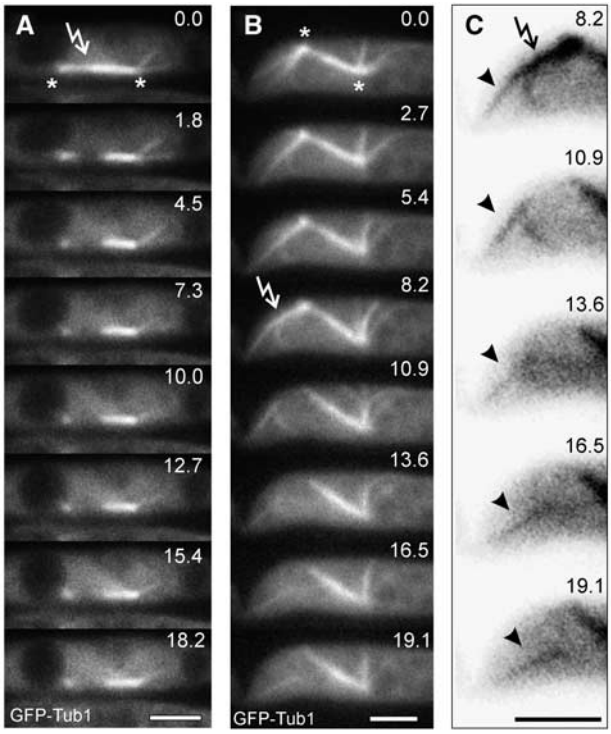

Figure 6 External pulling forces are absent in the dynein mutant. (**A**) Time series illustrating spindle pole separation after laser dissection in the temperature sensitive dynein mutant (FB1Dyn2^{ts}_GT) under restrictive conditions. This behavior was observed in all cases observed ($n = 10$). Elapsed time is given in seconds. Arrow indicates laser irradiation and asterisks the spindle poles. Bar: 3 μm. (**B**) Laser dissection of astral MTs in the dynein mutant under restrictive conditions. This behavior was observed in all cases observed ($n = 6$). Elapsed time is given in seconds. Arrow indicates laser irradiation and asterisks the spindle poles. Bar: 3 μm. (**C**) Detailed image series taken from (B). Arrow indicates laser irradiation, cut astral MT is indicated by arrowhead. Elapsed time is given in seconds. Bar: 3 μm.

MT (Figure 7D, arrowhead, asterisk marks plus end of the MT). This dynamic behavior suggests that dynein is constantly delivered to the MT tip by motor-based mechanisms, a notion that is supported by the observation that kinesin-1 participates in dynein targeting in interphase hyphae of *U. maydis* (Lenz *et al*, 2006). Interestingly, after cutting the distal MT with a laser or by an accidental breakage of the leading MT (Figure 7E; see Supplementary Movie 8), a new, long, leading MT rapidly established, immediately accumulated a large amount of dynein, and moved towards the cell pole (Figure 7E; asterisk), again demonstrating that outward forces are exerted by this leading MT (compare to Figure 1C). This is most likely a controlled process, as the signal intensities at the tip of distal MTs were not a function of the length of the MT (Figure 7F). The dynein signal was dispersed along the moving MT fragment, which suggests that the MT slides along dynein released from the tip. Taken together, these results indicate that dynein accumulates mainly at the tip of the distal leading MT, where it might participate in MT stabilization. However, this dynein signal is not stationary, but is constantly moving towards and away from the MT end.

Dynein appears to be off-loaded to the cortex during cortical sliding of MTs

In the yeast *S. cerevisiae* dynein is 'off-loaded' from the tip of astral MTs to the cortex, where it exerts force on the spindle (Lee *et al*, 2003; Sheeman *et al*, 2003). We searched for indications for such a mechanism in *U. maydis* and found that ~ 65% ($n = 54$) of all cortical MT sliding in anaphase occurred along stationary dynein signals (Figure 8A and B; see Supplementary Movie 9), which varied in their intensity. The data described above indicated that all MT sliding is based on dynein, suggesting that we did not detect dynein in the remaining 35% MT sliding. The stationary dynein was usually released from the large amount of accumulated dynein at the MT tip (Figure 8C), which suggested that dynein is 'off-loaded' to the cortex and exerts pulling forces

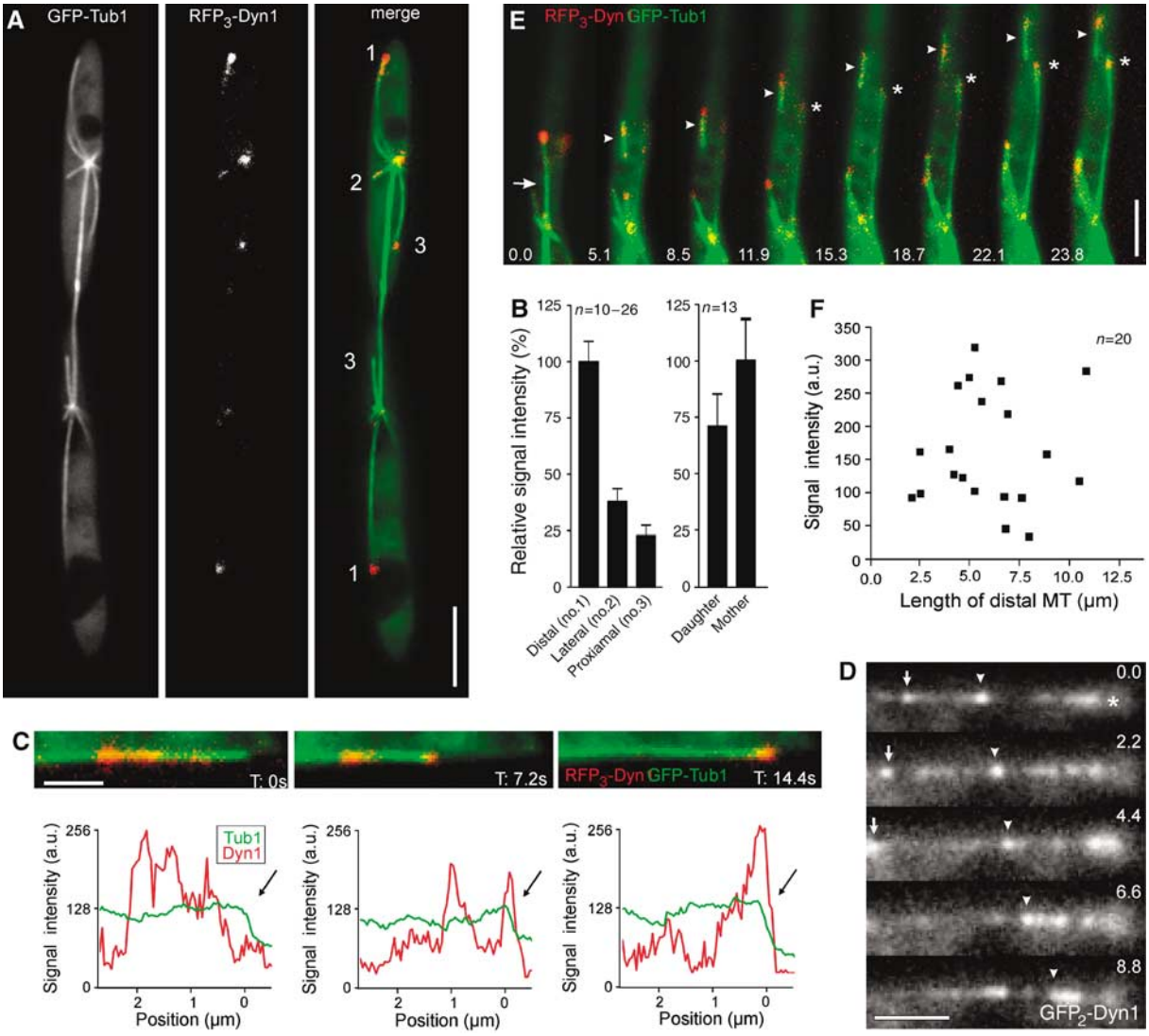

Figure 7 Dynamic behavior of dynein at plus-ends of distal MTs in *Ustilago maydis*. (**A**) Dynein localization at plus-ends of astral MTs in strain FB2R$_3$Dyn1_GT. The fluorescence of GFP-tagged spindles (GFP-Tub1), RFP-tagged dynein (RFP$_3$-Dyn1), and both together (merge) are shown. Astral MTs point in different directions (1: distal; 2: lateral; 3: proximal). Bar 5 μm. (**B**) Signal intensity measurements of RFP$_3$-Dyn1 at tips of astral MTs. The average intensity at the center of the dynein accumulation was measured using MetaMorph. Values are given as mean ± standard error of the mean. (**C**) Intensity profiles of dynein (RFP$_3$-Dyn1; red) located at the tip of a distal MT (GFP-α-tubulin; green) at the time points indicated. The corresponding signals are presented above each profile. The tip of the MT is indicated by arrows. Bar: 1 μm. (**D**) Bidirectional motility of GFP$_2$-Dyn1 along an astral MT. Signals are indicated by arrow and arrowhead, the MT plus-end is marked by asterisk. Time is given in seconds. Bar: 2 μm. (**E**) Establishment of a new leading MT (asterisk) after spontaneous breakage of the distal MT. Arrow indicates breakage of the MT; arrowhead indicate the fragment of the distal MT. Elapsed time in seconds is indicated. Bar: 5 μm. (**F**) Quantitative analysis of the relation between the length of the distal MT and the average dynein intensity at its tip. No linearity between the amount of dynein and the MT length was found, indicating that the strong accumulation at distal MTs is not due to more dynein targeting as a result of the increased length of these MTs.

Table II Microtubule dynamics and plus-end located dynein

Dynein	Elongation (μm min^{-1})	Depolymerization (μm min^{-1})	Catastrophe[a] (events min^{-1})	Rescue[b] (events min^{-1})	Pausing[c] (% of time)
No or faint signal	7.9 ± 2.2[d]	22.6 ± 14.9[e]	1.01 ± 0.15	0.86 ± 0.39	3.39 ± 0.62
Strong signal	7.8 ± 1.8[e]	22.6 ± 12.7[e]	1.66 ± 0.63	1.34 ± 0.24	7.34 ± 0.29

[a]3 experiments, each data set 26 microtubules.
[b]3 experiments, each data set 22 microtubules.
[c]2 experiments, each data set 35 microtubules.
[d]13 microtubules.
[e]11 microtubules.

on the spindle pole by minus-end directed motility along the distal MT.

Discussion

Rapid spindle elongation in U. maydis coincides with the appearance of long distal MTs

Anaphase in *U. maydis* starts with a phase of slow spindle elongation, in which chromosomes are separated and that might therefore be considered anaphase A. During this phase only short astral MTs are present that contact the cellular cortex. At the onset of anaphase B, longer astral MTs appeared and one distal MT was established at each spindle pole that reached 6–8 μm in length. The distal MTs exhibited reduced dynamic instability, and speckle analysis demonstrated that they slide along the cortex during spindle positioning and spindle elongation. Our nanosurgery experiments showed that the distal MTs exert forces on the spindle, which most likely participate in the four-fold increase in spindle elongation rate at the onset of anaphase B. Such forces exerted via astral MTs have been reported in *Caenorhabditis elegans* (Grill *et al*, 2001, 2003) *Nectria haematococca* (Aist and Berns, 1981; Aist *et al*, 1991). Surprisingly, severing the distal MT in *U. maydis* cells led to only short displacements, and the balance of forces applied on the spindle was rapidly restored. Indeed, we show here that a new long distal MT is rapidly established after loss of the leading MT. Furthermore, our nanosurgery experiments demonstrate that individual spindle halves undergo bidirectional movements and pauses. This indicates that opposing forces are applied on a single spindle pole (Figure 9; blue arrows indicate forces), which might be responsible for the positioning of the spindle poles in the center of the mother and daughter cell. If this is correct, some spatial information exists that affects the forces applied on the spindle poles. It will be a fascinating future challenge to elucidate this mechanism in *U. maydis*.

Kinesin-5 supports slow spindle elongation

In many other organisms, including the fungi *S. cerevisiae* and *S. pombe*, anaphase is mediated by the bi-polar tetrameric kinesin-5, which localizes to the mid-zone (Hagan and Yanagida, 1990), where it is thought to crosslink MTs (Kashina *et al*, 1997). *U. maydis* contains a member of the kinesin-5 family of proteins (Schuchardt *et al*, 2005). Temperature-sensitive *kin5*^{ts} single and *dyn2*^{ts}*kin5*^{ts} double mutants arrest in early mitosis, which suggests that Kin5 generates outward forces in anaphase A. Interestingly, in dynein mutants internal forces elongate spindles up to 8 μm, which corresponds well with the localization of Kin5 at the mid-zone of anaphase B spindles. This indicates that kinesin-5 not only provides outward forces for anaphase A but also cooperates with dynein during rapid anaphase B (Figure 9). Surprisingly, spindles still elongate in the *dyn2*^{ts} *kin5*^{ts} double mutants. It is presently unclear whether this reflects some residual activity of the temperature sensitive *kin5*^{ts} allele, or whether additional mechanisms participate in spindle elongation.

Dynein supports anaphase B by exerting force and reducing dynamic instability

Our data demonstrated that slow elongation in anaphase occurs independently of dynein, while anaphase B requires dynein, as well as dynactin. Consequently, we found that dynein was absent from short spindles, and only transiently appeared at the plus-ends of astral MTs when the spindle rotated. However, dynein accumulated at MT tips when long astral MTs formed at the onset of anaphase B. These long distal MTs carried the most dynein, were less dynamic, and slid along the cortex. It has been

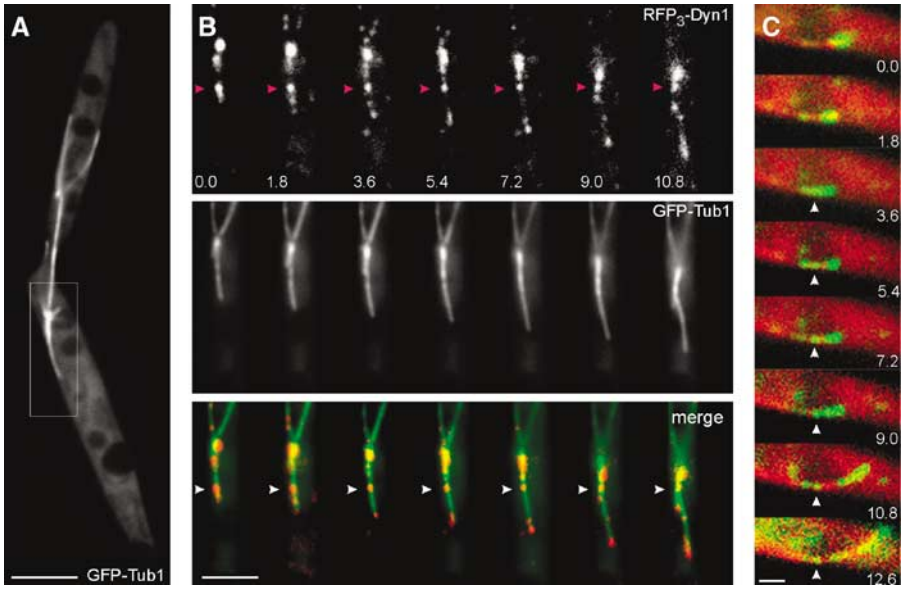

Figure 8 'Off-loading' of dynein during cortical sliding of astral MTs in *U. maydis*. (**A**) Mitotic cell of strain FB2GT, illustrating the sliding event shown in Figure 7B. Bar: 5 μm. (**B**) Dynein behavior during cortical MT sliding in strain FB2R$_3$Dyn1_GT. RFP$_3$-Dyn1 initially localizes to the tip of a GFP-labeled distal MT (GFP-Tub1). Arrowheads mark stationary dynein. Elapsed time in seconds is indicated. Bar: 3 μm. (**C**) In this example, the dynein complex is double tagged with GFP fused to the N-terminus of the endogenous Dyn1, and MTs are labeled by RFP-α-tubulin. Some dynein appears to be 'off-loaded' at the cortex and the MT slides along this signal (arrowheads) (strain FB2G$_2$Dyn1_RT). Elapsed time in seconds is indicated. Bar: 1 μm.

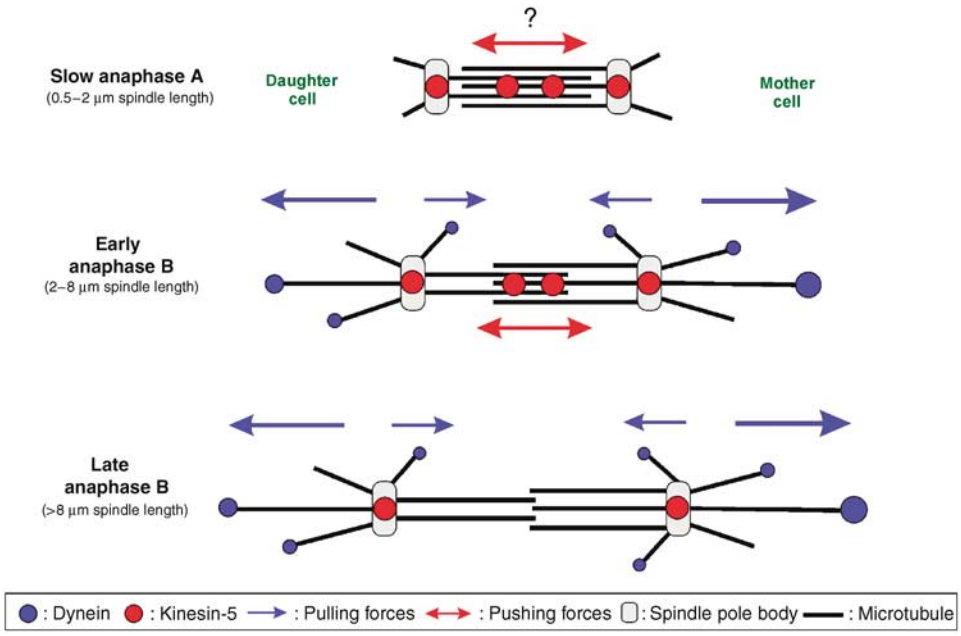

Figure 9 Motors in anaphase in *U. maydis*. In anaphase A, slow spindle elongation is supported by internal forces that might be generated by kinesin-5 localized at the mid-zone. Kinesin-5 also accumulates at the cell poles. Astral MTs in anaphase A are short and no dynein is located at their ends, except during rare rotational motion. When the spindle reaches a length of 1.5–2 µm, long astral MTs appear that carry dynein at their plus-end. Interestingly, more dynein is found at the tip of MTs that extend into the mother, which nicely corresponds to the faster velocity of spindle halves moving into the mother after laser dissection. Both spindle halves occasionally undergo bidirectional motility, which indicates that counteracting forces are applied on each individual spindle pole (blue arrows). The appearance of long astral MTs coincides with a four-fold increase in spindle elongation rate in early anaphase B. Dynein mutants fail to establish long distal MTs and the elongation rate does not increase, which suggests that dynein pulls on the spindle poles. In addition, kinesin-5 localizes at the mid-zone in anaphase B and seems to support spindle elongation up to 7–8 µm in dynein mutants, which indicates that it participates in spindle elongation. Kinesin-5 then disappears from the mid-zone, while dynein still pulls on the poles in late anaphase B. Note that additional forces might participate in anaphase A (indicated by ?).

previously described that dynein regulates interphase MT dynamics in *U. maydis* (Adamikova *et al*, 2004). It is therefore likely that dynein also modifies mitotic MTs and thereby participates in the formation of the distal, long MTs. This idea is supported by the observation that dynein mutants fail to establish long distal MTs, but nucleate numerous highly dynamic MTs that cannot establish contact with the cellular cortex. Thus, we conclude that dynein supports anaphase in two ways: (1) It modifies MT dynamics in order to establish a distal MT and (2) it mediates spindle elongation and positioning by pulling on these MTs. Consequently, dynein mutants fail to segregate their chromosomes, accumulate nuclei, which finally leads to death (Straube *et al*, 2001). Presently, the role of dynein in modifying MT dynamics in anaphase is not understood. However, the importance of this function is illustrated by the observation that chemical stabilization of MTs by low concentration of benomyl (1–1.5 µM; Adamikova *et al*, 2004) partially overcomes the lethal chromosome segregation defect (our unpublished results).

The dynein signal at plus-ends is dynamic and off-loaded during sliding

In *S. cerevisiae*, dynein positions the spindle in the neck region (Yeh *et al*, 2000). It has been suggested that this is achieved by an 'off-loading' mechanism, in which dynein located at the plus-end is taken to the cortex, where it becomes activated and off-loaded (Lee *et al*, 2003; Sheeman *et al*, 2003). While anchored at the cell cortex, the minus-end directed transport activity of dynein exerts force on the astral MT, thereby pulling on the MT. In *U. maydis*, dynein also concentrated at the tip of the sliding distal MT, and we found evidence for a dynamic rearrangement of dynein during sliding. It has been reported that organelles show rapid bidirectional transport along astral MTs in mitosis (Aist and Bayles, 1991), which raises the possibility that part of the dynein departure is due to retrograde membrane traffic. However, we also find that dynein remains stationary at the cortex during MT sliding. This observation clearly supports the 'off-loading' concept and suggests that the same mechanism supports cortical MT sliding during rapid spindle elongation in anaphase B in *U. maydis*.

Different mechanisms of fungal spindle elongation depending on cell length

Much of our knowledge about the role of motors in anaphase comes from studies on the yeasts *S. cerevisiae* and *S. pombe*. In both yeasts, kinesin-5 powers slow elongation of the anaphase spindle (Hagan and Yanagida, 1990; Hoyt *et al*, 1992), whereas dynein has no obvious role in anaphase (Saunders *et al*, 1995; Yeh *et al*, 1995). In *U. maydis*, initial spindle elongation is also slow and requires kinesin-5, indicating that a kinesin-5-based mechanism is generally used to in fungal anaphase. However, in contrast to both yeasts, spindle elongation in *U. maydis* requires dynein pulling on astral MTs. This is reminiscent of the situation in *D. melanogaster* (Sharp *et al*, 2000) and *C. elegans* (Tu Nguyen-Ngoc and Pierre Gönczy, personal communication), which suggests that a role of dynein in spindle elongation has been evolutionarily conserved in animals and fungi. But why was this mechanism lost in *S. cerevisiae* and *S. pombe*? An obvious difference between *U. maydis* and both yeasts is

the cell size. Mitotic cells of *S. cerevisiae* have an average length of 11.5 μm (our own unpublished data) and *S. pombe* reaches 13.2 μm (Mitchison and Nurse, 1985). Both yeasts form spindles of 8–13 μm in length and are in anaphase for 8–10 min (Yeh *et al*, 1995) or 8.6 min (Hagan and Yanagida, 1990). In contrast, *U. maydis* cells reach at average cell length of 31 μm (our own unpublished data), which requires a spindle length of at least 20–25 μm in order to segregate the DNA. Consequently, a slow kinesin-5-based elongation mechanism would keep the cell in anaphase for at least 15–17 min. The use of dynein significantly accelerated anaphase, as this phase lasts only ~3.5 min (Straube *et al*, 2005). Although the gain in time is just ~11–13 min, this results in an ~9–10% decrease in doubling time, which might be a significant advantage in the competition for resources. In other words, it is possible that the larger dimensions of *U. maydis* cells are responsible for the conservation of the use of dynein in spindle elongation.

Materials and methods

Strains and plasmids

The genotypes of the *U. maydis* strains and plasmids used in this study are summarized in Table I. Strains FB1GT and FB2GT contain an ectopic copy of GFP-α-tubulin (Steinberg *et al*, 2001). In strains FB2rGFPTub1, FB2rDya1_GT and FB1rDyn2_GT expression of GFP-α-tubulin fusion protein, the *dyn2* gene which encodes the C-terminal half of the dynein heavy chain (Straube *et al*, 2001) or the p150 subunit of the dynactin complex (Lenz *et al*, 2006) was under the control of the glucose-repressible *crg* promoter (Bottin *et al*, 1996). Dynein was visualized fusing triple RFP ($FB2R_3Dyn1\_GT$) or a double GFP ($FB2G_2Dyn1\_RT$) to the 5′ end of the endogenous *dyn1* gene, which encodes the N-terminal half of the dynein heavy chain (Straube *et al*, 2001). In addition, MTs were labeled by ectopic expression of GFP-α-tubulin or RFP-α-tubulin. Strain $FB2G_3Kin5$ contained a triple GFP tag fused to the N-terminus of the endogenous *kin5* gene. Chromosome separation in early anaphase was monitored using genomic DNA labeled with histone-4 fused to cyan-shifted fluorescent protein (CFP); MTs were labeled with yellow-shifted fluorescent protein (YFP)-α-tubulin (FB1H4C_YT; Straube *et al*, 2005). The conditional mutant strain $FB1Dyn2^{ts}\_GT$ (Adamikova *et al*, 2004) contains a temperature-sensitive mutant allele of *dyn2* (Wedlich-Soldner *et al*, 2002). Strains $AB33Kin5^{ts}\_GT$, $FB1Kin5^{ts}\_Tub2G$ and $FB1Dyn2^{ts}\_Kin5^{ts}\_GT$ were generated by introducing a point mutation (R210K) by PCR in the motor domain of *kin5*; this mutation confers temperature sensitivity to *CIN8* of *S. cerevisiae* (Gheber *et al*, 1999). All genomic (homologous) integrations were confirmed by Southern blot analysis. DNA isolation and construction of plasmids followed standard protocols. *U. maydis* was transformed as described previously (Schulz *et al*, 1990).

Growth conditions

Strains were cultivated at 28°C on solid medium containing 2% (w/v) bacto-agar and supplemented with 1% glucose or 1% arabinose. For light microscopy, strains were grown overnight at 28°C in liquid complete medium (CM; Holliday, 1974) supplemented with 1% glucose (CM-G) or 1% arabinose (CM-A) with shaking at 200 r.p.m. For repression of the inducible *crg* promoter in strains FB2rGT, FB1rDyn2_GT and FB2rDya_GT, cells were either grown over night in CM-A and shifted for 28–36 h in CM-G or directly inoculated in CM-G. Temperature-sensitive dynein and kinesin-5 strains were grown in CM-G at 200 r.p.m. at 22 and 16°C, respectively. Motors were inactivated by shifting mutant cells to 32°C for 2–4 h.

Light microscopy and speckle analysis

Exponentially growing cells were placed on a 2% agar cushion and immediately observed using a Zeiss Axioplan II imaging microscope (Oberkochen, Germany) and fluorescent filters as previously described (Straube *et al*, 2005). In co-localization experiments, image sequences of 30–40 frames were taken at an exposure time of 800–900 ms. For the observation of dynamics and sliding of GFP-α-tubulin-labeled MTs, images series of 60–120 frames at 500 ms were taken. A CoolSNAP-HQ CCD camera (Photometrics, Tucson, Ariz., USA) controlled by the imaging software Metamorph (Universal Imaging, Downingtown, PA, USA) was used.

Speckle analysis was performed as described (Straube *et al*, 2006). Briefly, strain FB2rGFPTub1 (Steinberg *et al*, 2001) was grown in CM-A, in which cells expressed an additional copy of α-tubulin fused to GFP under the control of the *crg* promoter. After shift to CM-G, the glucose in the medium represses the expression of the fusion protein, leading to a gradual decrease in the amount of the protein in the cells. This leads to speckles within the MT after ~4 h.

Microtubule surgery

Microtubules were severed as previously described (Colombelli *et al*, 2004) using a pulsed UV laser coupled to a conventional inverted Zeiss microscope (Oberkochen, Germany). MT breakage was induced by an energy pulse of 50–200 nJ and a linear density distribution of laser pulses of 5.5 pulses per micron along the manually defined laser line path and a laser frequency ranging from 100 to 1000 Hz.

Quantitative analysis

Microtubule length changes during MT sliding were measured in image sequences of 40–60 frames. Microtubule dynamics was quantitatively analyzed as described previously (Steinberg *et al*, 2001). Metamorph software was used to measure the fluorescence signal of RFP-Dyn2 at the astral MT plus-end in images taken at the same exposure time and light intensity. MT plus-ends were determined in randomly taken images sequences; dynein intensities at these MT tips were measured only in the first image in order to avoid bleaching artifacts. 'Off-loaded' stationary dynein signals were counted as such if no motion was observed for at least three frames of MT sliding, and their intensity was determined in the first frame. Elongation rates were measured on GFP-α-tubulin-labeled spindles at different time points in images series of 30 s duration. These data were summarized in a graph and analyzed by linear regression using the software PRISM (GraphPad, San Diego, CA, USA). Speckles were also line-scan analyzed using Metamorph. All images were processed and brightness, contrast and gamma values were adjusted using Metamorph and Adobe Photoshop. Statistical analysis by two-tailed *t*-test at $\alpha = 0.05$ and linear regression was carried out using PRISM (GraphPad). All values are given as means ± standard deviation unless otherwise stated.

Staining procedures

CFP-labeled histone-4 and YFP-tagged spindles were used for correlating chromosome separation and spindle length. Cells were mildly fixed with formaldehyde (stock solution 16%, EM-grade, Polyscience) added to growing cultures to a final concentration of 1%. This treatment preserved the GFP-label on the MTs. DNA was stained with DAPI as previously described (Straube *et al*, 2001). Colocalization studies of GFP-γ-tubulin and MTs were performed by immunofluorescence as previously described (Steinberg *et al*, 2001).

Supplementary data

Supplementary data are available at *The EMBO Journal* Online (http://www.embojournal.org).

Acknowledgements

This work was supported by the Deutsche Forschungsgemeinschaft, Ste 799-4. We are grateful to Karen Brune for improving the manuscript.

References

Adamikova L, Straube A, Schulz I, Steinberg G (2004) Calcium signaling is involved in dynein-dependent microtubule organization. *Mol Biol Cell* **15:** 1969–1980

Aist JR, Bayles CJ (1991) Organelle motility within mitotic asters of the fungus *Nectria haematococca*. *Eur J Cell Biol* **56:** 358–363

Aist JR, Bayles CJ, Tao W, Berns MW (1991) Direct experimental evidence for the existence, structural basis and function of astral forces during anaphase B *in vivo*. *J Cell Sci* **100** (Part 2)**:** 279–288

Aist JR, Berns MW (1981) Mechanics of chromosome separation during mitosis in Fusarium (Fungi imperfecti): new evidence from ultrastructural and laser microbeam experiments. *J Cell Biol* **91:** 446–458

Aist JR, Liang H, Berns MW (1993) Astral and spindle forces in PtK2 cells during anaphase B: a laser microbeam study. *J Cell Sci* **104** (Part 4)**:** 1207–1216

Barton NR, Goldstein LS (1996) Going mobile: microtubule motors and chromosome segregation. *Proc Natl Acad Sci USA* **93:** 1735–1742

Bottin A, Kamper J, Kahmann R (1996) Isolation of a carbon source-regulated gene from *Ustilago maydis*. *Mol Gen Genet* **253:** 342–352

Colombelli J, Grill SW, Stelzer EHK (2004) Ultraviolett diffraction limited nanosurgery of live biological tissues. *Rev Sci Instr* **75:** 472–478

Colombelli J, Reynaud EG, Rietdorf J, Pepperkok R, Stelzer EH (2005) *In vivo* selective cytoskeleton dynamics quantification in interphase cells induced by pulsed ultraviolet laser nanosurgery. *Traffic* **6:** 1093–1102

Drummond DR, Hagan IM (1998) Mutations in the bimC box of Cut7 indicate divergence of regulation within the bimC family of kinesin related proteins. *J Cell Sci* **111** (Part 7)**:** 853–865

Gadde S, Heald R (2004) Mechanisms and molecules of the mitotic spindle. *Curr Biol* **14:** R797–R805

Gheber L, Kuo SC, Hoyt MA (1999) Motile properties of the kinesin-related Cin8p spindle motor extracted from *Saccharomyces cerevisiae* cells. *J Biol Chem* **274:** 9564–9572

Gönczy P (2002) Mechanisms of spindle positioning: focus on flies and worms. *Trends Cell Biol* **12:** 332–339

Grill SW, Gonczy P, Stelzer EH, Hyman AA (2001) Polarity controls forces governing asymmetric spindle positioning in the *Caenorhabditis elegans* embryo. *Nature* **409:** 630–633

Grill SW, Howard J, Schaffer E, Stelzer EH, Hyman AA (2003) The distribution of active force generators controls mitotic spindle position. *Science* **301:** 518–521

Grill SW, Hyman AA (2005) Spindle positioning by cortical pulling forces. *Dev Cell* **8:** 461–465

Hagan I, Yanagida M (1990) Novel potential mitotic motor protein encoded by the fission yeast cut7+ gene. *Nature* **347:** 563–566

Hagan I, Yanagida M (1992) Kinesin-related cut7 protein associates with mitotic and meiotic spindles in fission yeast. *Nature* **356:** 74–76

Helenius J, Brouhard G, Kalaidzidis Y, Diez S, Howard J (2006) The depolymerizing kinesin MCAK uses lattice diffusion to rapidly target microtubule ends. *Nature* **441:** 115–119

Hirokawa N (1998) Kinesin and dynein superfamily proteins and the mechanism of organelle transport. *Science* **279:** 519–526

Holliday R (1974) *Ustilago maydis*. In *Handbook of Genetics*, King RC (ed), Vol. 1, pp 575–595. New York, USA: Plenum Press

Hoyt MA, He L, Loo KK, Saunders WS (1992) Two *Saccharomyces cerevisiae* kinesin-related gene products required for mitotic spindle assembly. *J Cell Biol* **118:** 109–120

Karki S, Holzbaur EL (1999) Cytoplasmic dynein and dynactin in cell division and intracellular transport. *Curr Opin Cell Biol* **11:** 45–53

Kashina AS, Rogers GC, Scholey JM (1997) The bimC family of kinesins: essential bipolar mitotic motors driving centrosome separation. *Biochim Biophys Acta* **1357:** 257–271

Khodjakov A, La Terra S, Chang F (2004) Laser microsurgery in fission yeast; role of the mitotic spindle midzone in anaphase B. *Curr Biol* **14:** 1330–1340

Lee WL, Oberle JR, Cooper JA (2003) The role of the lissencephaly protein Pac1 during nuclear migration in budding yeast. *J Cell Biol* **160:** 355–364

Lenz JH, Schuchardt I, Straube A, Steinberg G (2006) A dynein loading zone for retrograde endosome motility at microtubule plus-ends. *EMBO J* **25:** 2275–2286

Mitchison JM, Nurse P (1985) Growth in cell length in the fission yeast *Schizosaccharomyces pombe*. *J Cell Sci* **75:** 357–376

Moore A, Wordeman L (2004) The mechanism, function and regulation of depolymerizing kinesins during mitosis. *Trends Cell Biol* **14:** 537–546

Noda Y, Okada Y, Saito N, Setou M, Xu Y, Zhang Z, Hirokawa N (2001) KIFC3, a microtubule minus end-directed motor for the apical transport of annexin XIIIb-associated Triton-insoluble membranes. *J Cell Biol* **155:** 77–88

O'Connell CB, Wang YL (2000) Mammalian spindle orientation and position respond to changes in cell shape in a dynein-dependent fashion. *Mol Biol Cell* **11:** 1765–1774

Saunders WS, Koshland D, Eshel D, Gibbons IR, Hoyt MA (1995) *Saccharomyces cerevisiae* kinesin- and dynein-related proteins required for anaphase chromosome segregation. *J Cell Biol* **128:** 617–624

Schuchardt I, Assmann D, Thines E, Schuberth C, Steinberg G (2005) Myosin-V, Kinesin-1, and Kinesin-3 cooperate in hyphal growth of the fungus *Ustilago maydis*. *Mol Biol Cell* **16:** 5191–5201

Schulz B, Banuett F, Dahl M, Schlesinger R, Schafer W, Martin T, Herskowitz I, Kahmann R (1990) The b alleles of *U. maydis*, whose combinations program pathogenic development, code for polypeptides containing a homeodomain-related motif. *Cell* **60:** 295–306

Sharp DJ, Brown HM, Kwon M, Rogers GC, Holland G, Scholey JM (2000) Functional coordination of three mitotic motors in *Drosophila* embryos. *Mol Biol Cell* **11:** 241–253

Sharp DJ, McDonald KL, Brown HM, Matthies HJ, Walczak C, Vale RD, Mitchison TJ, Scholey JM (1999) The bipolar kinesin, KLP61F, cross-links microtubules within interpolar microtubule bundles of *Drosophila* embryonic mitotic spindles. *J Cell Biol* **144:** 125–138

Sharp DJ, Rogers GC (2004) A Kin I-dependent Pacman-flux mechanism for anaphase A. *Cell Cycle* **3:** 707–710

Sheeman B, Carvalho P, Sagot I, Geiser J, Kho D, Hoyt MA, Pellman D (2003) Determinants of *S. cerevisiae* dynein localization and activation: implications for the mechanism of spindle positioning. *Curr Biol* **13:** 364–372

Steinberg G, Wedlich-Soldner R, Brill M, Schulz I (2001) Microtubules in the fungal pathogen *Ustilago maydis* are highly dynamic and determine cell polarity. *J Cell Sci* **114:** 609–622

Straube A, Enard W, Berner A, Wedlich-Soldner R, Kahmann R, Steinberg G (2001) A split motor domain in a cytoplasmic dynein. *EMBO J* **20:** 5091–5100

Straube A, Brill M, Oakley BR, Horio T, Steinberg G (2003) Microtubule organization requires cell cycle dependent nucleation at dispersed cytoplasmic sites, polar and perinuclear MTOCs in the plant pathogen *Ustilago maydis*. *Mol Biol Cell* **14:** 642–657

Straube A, Hause G, Fink G, Steinberg G (2006) Conventional Kinesin mediates microtubule-microtubule interactions *in vivo*. *Mol Biol Cell* **17:** 907–916

Straube A, Weber I, Steinberg G (2005) A novel mechanism of nuclear envelope break-down in a fungus: nuclear migration strips off the envelope. *EMBO J* **24:** 1674–1685

Tolic-Norrelykke IM, Sacconi L, Thon G, Pavone FS (2004) Positioning and elongation of the fission yeast spindle by microtubule-based pushing. *Curr Biol* **14:** 1181–1186

Vaisberg EA, Koonce MP, McIntosh JR (1993) Cytoplasmic dynein plays a role in mammalian mitotic spindle formation. *J Cell Biol* **123:** 849–858

Wedlich-Soldner R, Straube A, Friedrich MW, Steinberg G (2002) A balance of KIF1A-like kinesin and dynein organizes early endosomes in the fungus *Ustilago maydis*. *EMBO J* **21:** 2946–2957

Yamamoto A, West RR, McIntosh JR, Hiraoka Y (1999) A cytoplasmic dynein heavy chain is required for oscillatory nuclear movement of meiotic prophase and efficient meiotic recombination in fission yeast. *J Cell Biol* **145:** 1233–1249

Yeh E, Skibbens RV, Cheng JW, Salmon ED, Bloom K (1995) Spindle dynamics and cell cycle regulation of dynein in the budding yeast, *Saccharomyces cerevisiae*. *J Cell Biol* **130:** 687–700

Yeh E, Yang C, Chin E, Maddox P, Salmon ED, Lew DJ, Bloom K (2000) Dynamic positioning of mitotic spindles in yeast: role of microtubule motors and cortical determinants. *Mol Biol Cell* **11:** 3949–3961

Zhu C, Zhao J, Bibikova M, Leverson JD, Bossy-Wetzel E, Fan JB, Abraham RT, Jiang W (2005) Functional analysis of human microtubule-based motor proteins, the kinesins and dyneins, in mitosis/cytokinesis using RNA interference. *Mol Biol Cell* **16:** 3187–3199

